Available online at www.sciencedirect.com
SCIENCE DIRECT®
Combustion and Flame 137 (2004) 506–522
Combustion and Flame
www.elsevier.com/locate/jnlabr/cnf

Suppression of cup-burner flames using carbon dioxide in microgravity

V.R. Katta,[a,*] F. Takahashi,[b] and G.T. Linteris [c]

[a] *Innovative Scientific Solutions Inc., 2766 Indian Ripple Road, Dayton, OH 45440, USA*
[b] *National Center for Microgravity Research on Fluids and Combustion, NASA Glenn Research Center, 21000 Brookpark Road, Cleveland, OH 44135, USA*
[c] *Fire Research Division, National Institute of Standards and Technology, Gaithersburg, MD 20899, USA*

Received 22 April 2003; received in revised form 20 November 2003; accepted 21 January 2004

Available online 9 April 2004

Abstract

The extinguishment characteristics of CO_2 as a fire-suppressing agent have been studied experimentally and numerically using a methane–air laminar co-flow diffusion flame stabilized on a cup burner. Direct numerical simulations of cup-burner flames under various gravitational forces were performed using a time-dependent, axisymmetric mathematical model with a detailed-chemical-kinetic mechanism for CH_4/O_2 combustion. Experiments with cup-burner flames under normal-gravity ($1g$) conditions were performed for comparison purposes. Both the computed flicker frequency and the predicted critical concentration of CO_2 for extinguishing the flame compared well with the respective quantities measured in the experiments. As the buoyancy force is reduced, the flicker frequency decreases, the flame diameter increases, the tip opens, and the base becomes vertical. It is predicted that the cup-burner flame ceases to flicker for gravitational forces corresponding to less than $0.5g$. Numerical experiments revealed that radiative heat loss is predominantly responsible for flame quenching (opening) in the tip region under microgravity ($0g$) conditions. In contrast, $1g$ flames are affected only slightly by the radiative heat loss. Calculations are made by adding different amounts of CO_2 to the air stream for obtaining the critical volume fraction of CO_2 to extinguish $0g$ flames. The behavior is similar to that observed in $1g$ flames: the addition of CO_2 destabilizes the flame base, which then moves downstream in search of a new stabilization location. For CO_2 volume fractions greater than 19.1%, the flame base moves out of the computational area, as it cannot find a stabilization point within the domain. This critical concentration for the $0g$ flames is $\sim 32\%$ higher than that computed for the same flames under $1g$ conditions. Calculations made by ignoring radiation for the limiting flame under $0g$ conditions yielded a stable flame. This study suggests that it is important to consider radiation heat losses when estimating the extinguishment limits of cup-burner flames in microgravity.

Keywords: Fire-safety; Fire-suppression; Extinguishment; Buoyancy; Inhibitors; Cup-burner

1. Introduction

A fire, either within a spacecraft or in an occupied space on extraterrestrial bases, can lead to mission termination and/or loss of life. The advent of longer duration missions to the moon, to Mars, or aboard a space station increases the likelihood of mishaps that result from fire. Therefore, development of efficient fire-safety systems and procedures for use in spacecraft environments represents a mission-critical task. Chemically active agents such as trifluorobro-

* Corresponding author. Fax: (937)-255-3139.
E-mail address: vrkatta@innssi.com (V.R. Katta).

0010-2180/$ – see front matter
doi:10.1016/j.combustflame.2004.01.015

momethane (CF_3Br, Halon 1301) are widely used for both terrestrial and spacecraft applications [1], and numerous studies have been conducted in attempts to understand their inhibition mechanism [2–5]. Unfortunately, as halons deplete stratospheric ozone, their use is likely to be reduced in the future. Furthermore, because typical HVAC systems on spacecraft cannot easily remove the agents from the environment after the fire is extinguished, halons are unlikely to be used on long-duration space missions. The predominantly inert agent CO_2 was considered in the present study mainly because of (1) its wide use on earth and (2) its choice as the suppressant in the U.S. modules of the International Space Station. Also, understanding the suppression mechanisms of CO_2 (and other inert agents) as well as CF_3Br is important for their efficient usage and for the development of new ones.

Studies to gain an understanding of the inhibiting effects of fire suppressants on flames have been performed in premixed [6–8] and diffusion [9–11] systems. Premixed flames have been selected mainly because the overall reaction rate, heat release, and heat and mass transport in these flames can be described with a single fundamental parameter—the laminar burning velocity. On the other hand, most common fires are of the diffusion (non-premixed) type and often, under the influence of earth's gravitational force, become dynamic in nature, with large vortical structures entraining additional surrounding air.

The predominant laboratory-scale experimental techniques for studying fire suppression in non-premixed flames employ either laminar co-flow diffusion flames formed on a cup burner [12] or the opposing-jet configuration. In both of these experiments, agents are quasi-statically added to either the fuel or the air stream. The opposing-jet configuration offers very simple flames that can be modeled using one-dimensional analysis and, hence, is often used for the development of chemical-kinetic models for various agents. From a fire-safety point of view, however, the most hazardous situation is a low-strain-rate diffusion flame such as those established over a cup burner; these flames are more stable and larger concentrations of the agent are required to extinguish them. Studies on cup-burner flames are also important because the amount of agent required to extinguish these flames is thought to scale to the requirements in common fires.

Under normal-gravity ($1g$) conditions, a laminar co-flow diffusion flame formed over a cup burner with a negligibly small fuel flow rate and a low-speed annular airflow will develop large-scale, low-frequency (1–40 Hz), organized buoyancy-induced vortices on the air side. Both experimental [13,14] and numerical [15] studies have been performed on cup-burner dynamic flames and steady, opposing-jet diffusion flames to identify the differences in the agent requirements for extinguishing these flames. On the other hand, several studies [16–18] have indicated that low-speed, coaxial, jet diffusion flames similar to those associated with cup-burners exhibit different behavior under microgravity ($0g$). As a result, the agent requirements for extinguishing the cup-burner flames in $0g$ could be different from those established in ground-based studies.

Several numerical investigations of dynamic jet flames using the conserved-scalar, global-chemistry, and detailed-chemistry models have elucidated important aspects of combustion such as the effect of heat release rate [19], the role of buoyancy [17,20], the enhancement of soot formation [21], and the effects of Lewis number [22,23]. The authors recently performed comprehensive computations for predicting the effects of various fire-suppressing agents [CO_2, CF_3H, and $Fe(CO)_5$] on methane jet diffusion flames in $1g$ using detailed chemical-kinetic mechanisms [15,24,25].

The present article describes an investigation performed for establishing the extinguishment criterion of cup-burner flames in microgravity. A two-dimensional numerical model with detailed kinetics that accurately simulates dynamic diffusion flames was employed. The capabilities of the numerical model were validated previously by simulating various steady-state and dynamic flames. For comparison, experiments were performed for the cup-burner flames under normal-gravity conditions. Carbon dioxide, added to the air stream, was employed as a fire-suppressing agent in both the experiments and the simulations. The extinguishment characteristics of CO_2 in cup-burner jet diffusion flames under normal-gravity conditions were compared with those obtained in counterflow diffusion flames. Finally, numerical experiments were performed in an attempt to understand the dramatic structural differences observed in cup-burner flames operating under normal-gravity, low-gravity, and microgravity conditions.

2. Experiment

The cup burner described previously [13–15] was used for the present investigations on the effects of gravity on flame extinguishment. The burner consists of a cylindrical glass cup (28 mm in diameter) positioned inside a glass chimney (53.3 cm in height, 9.5 cm in diameter). To provide uniform flow, the base of the chimney was filled with 6-mm glass beads, the fuel cup was filled with 3-mm glass beads, and the burner assembly was covered with two 15.8-mesh/cm screens. Gas flows were measured by mass flow con-

trollers (Sierra 860[1]) that were calibrated such that their uncertainty would be 2% of the indicated flow. (All uncertainties are expressed as expanded uncertainties, with a coverage factor of 2.) The flow rate of the co-flowing gas was held constant at 41.6 ± 0.8 L/min. For determining the extinguishment condition, CO_2 was added to the flow (in increments of $< 1\%$ near extinguishment), while the corresponding amount of co-flow air was reduced until liftoff was observed. The co-flow velocity with and without CO_2 was 10.7 ± 0.21 cm/s, and the fuel-jet velocity was 0.921 ± 0.018 cm/s. These velocities closely represent those of entraining air and evaporating fuel, respectively, of a liquid-fueled cup-burner flame. The test for each condition was repeated at least three times. The fuel gas used was methane (Matheson UHP, 99.9%); the agent was CO_2 (airgas); and the air was house compressed air (filtered and dried), which was additionally cleaned by passing it through an 0.01-μm filter, a carbon filter, and a desiccant bed to remove small aerosols, organic vapors, and water vapor. Visual flame images were recorded on VHS video tape using a charge-coupled-device (CCD) camera (512×512 pixels) and subsequently analyzed with image analysis software to determine the flame base location.

3. Computational model

A time-dependent, axisymmetric mathematical model known as UNICORN (Unsteady Ignition and Combustion using Reactions) [26] was used for the simulation of unsteady jet diffusion flames associated with the cup burner. This model solves for axial and radial (z and r) momentum equations, the continuity equation, and enthalpy- and species-conservation equations on a staggered-grid system. The body force term due to the gravitational field is included in the axial momentum equation to simulate upward-oriented flames. A clustered mesh system is employed to trace the gradients in flow variables near the flame surface. A detailed chemical-kinetic model GRI-V1.2 (developed by the Gas Research Institute) [27] is incorporated into UNICORN for investigation of the effects of CO_2 on methane combustion. This mechanism for methane flames is comprehensive, with 31 species and 346 elementary reactions. Thermophysical properties such as enthalpy, viscosity, thermal conductivity, and binary molecular diffusion of all of the species are calculated from the polynomial curve fits developed for the temperature range 300–5000 K. Mixture viscosity and thermal conductivity are then estimated using the Wilke and Kee expressions, respectively. Binary-type diffusion is assumed, with the diffusion velocity of a species being calculated using Fick's law and the effective-diffusion coefficient of that species in the mixture. A simple radiation model based on the optically thin medium assumption was incorporated into the energy equation. Only radiation from CO_2, H_2O, CO, and CH_4 was considered in the present study [28].

The finite-difference forms of the momentum equations are obtained using an implicit QUICKEST scheme [17], and those of the species and energy equations are obtained using a hybrid scheme of upwind and central differencing. At every time-step, the pressure field is accurately calculated by solving all of the pressure Poisson equations simultaneously and using the LU (lower and upper diagonal) matrix-decomposition technique.

Unsteady axisymmetric calculations for the cup-burner flames were made on a physical domain of 200×47.5 mm, using a 251×101 nonuniform grid system that yielded 0.2-mm grid spacing in both the z and r directions in the flame zone. The computational domain is bounded by the axis of symmetry and a chimney wall in the radial direction and by the inflow and outflow planes in the axial direction. The outer boundary in the z direction is located sufficiently far from the burner exit (~ 7.5 fuel-cup diameters) that propagation of boundary-induced disturbances into the region of interest is minimal. Flat velocity profiles are imposed at the fuel and air inflow boundaries, while an extrapolation procedure with weighted zero- and first-order terms is used to estimate the flow variables at the outflow boundary. Details of the boundary conditions are given in Ref. [29].

It is well known that heat transfer between the flame base and the burner rim plays a crucial role in the stability of the attached flames. For an accurate simulation of the flow structure at the base of the flame, the fuel-cup wall was treated as a 1-mm-long, 1-mm-thick tube in the calculations. Note that even though this millimeter-size wall may not be sufficient for capturing the base structure of a well-anchored diffusion flame, it is sufficient for the flames that are near extinguishment (near-lift-off conditions), which are the main focus of the present study. For simulating the heat transfer between the burner rim and the flame, the temperature of the tubular rim was set at 600 K, which is close to that estimated from the experiments.

The CFD model described above has been extensively validated in the past by simulating vari-

[1] Certain commercial equipment, instruments, or material are identified in this paper for adequately specifying the procedure. Such identification does not imply recommendation or endorsement by NIST, nor does it imply that the materials or equipment are necessarily the best available for the intended use.

ous steady and unsteady counterflow [30,31] and co-flow [17,32] jet diffusion flames and by comparing the results with experimental data. Flame-flicker characteristics [32], the flame liftoff process [33], and the gravitational effects on buoyant jet flames [17,26] have been successfully simulated. The velocities used in the previous studies on jet diffusion flames [26,32] are comparable to these employed in the cup burners, which builds confidence in the ability of the numerical model employed to simulate accurately the dynamic nature of the flames associated with cup burners.

Simulations for the cup-burner jet diffusion flames were performed on a Pentium III 1-GHz-based personal computer with 1 GB of memory. Typical execution time was ~ 52 s/time-step. Stably oscillating flames were obtained in about 3000 time-steps (which corresponds to 300 ms in real time).

4. Results and discussion

The uniform flow of non-premixed reactants in a cup-burner results in an axisymmetric, laminar diffusion flame. Typically, very low velocities are employed for the reactant flows in these burners to ensure that the flames generated are quite stable and that their structures are similar to those of uncontrolled fires. Under the influence of gravitational force, the low annular-air velocity promotes buoyancy-induced instabilities outside the flame surface and causes the flame to flicker at a low frequency. Several calculations were made in attempts to understand the structure and extinguishment characteristics of these dynamic flames under $1g$ conditions.

4.1. Flame dynamics under normal gravity

The co-flowing fuel and air velocities of 0.921 and 10.7 cm/s, respectively, used in the present investigation establish a weakly strained flame. The low fuel-jet velocity represents a condition, at which its flame size is comparable to that of liquid fuels in the cup burner. The airflow velocity is in the middle of the so-called "plateau region," where the critical CO_2 concentration at extinguishment is independent of the oxidizer velocity [24]. The computed instantaneous flowfield of the pure CH_4/air flame is shown in Fig. 1. The CO_2 iso-mole fraction and temperature distributions are shown on the left and right halves, respectively. The velocity and iso-contours of the H_2 mole fraction are superimposed on the temperature and CO_2 distributions, respectively. Except in the base region (0.1 mm $< z <$ 4 mm), the peak temperature of the flame is nearly constant everywhere at 1880 K. The flame height (the distance between the burner tip and the axial location at which the peak in

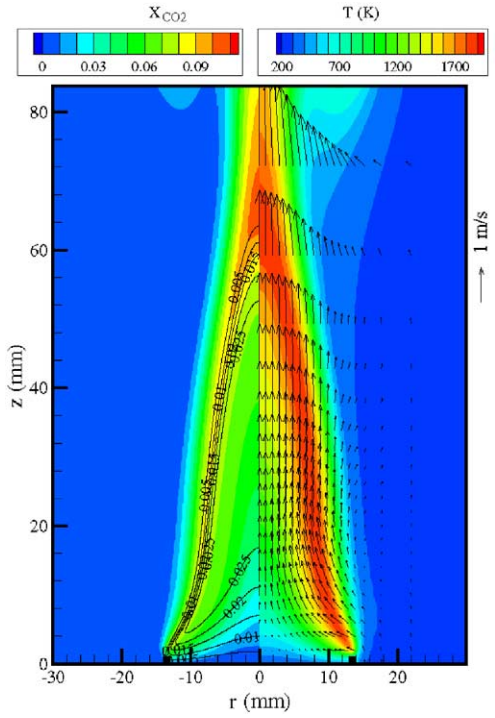

Fig. 1. Cup-burner flame simulated under normal-gravity conditions. Distributions of CO_2 mole fraction and temperature are plotted in left and right halves, respectively. Contours of H_2 mole fraction and velocity field are superimposed on left and right halves, respectively.

radial temperature distribution occurs at the centerline) at the instant shown in Fig. 1 is ~ 64 mm.

The striking features of this flame are (1) the low-frequency, large-amplitude oscillations in flame height, and (2) the significant inward inclination in the flame surface at the base. Because of the gravity term in the axial momentum equation and because of the low-speed annular-airflow (10.7 cm/s), solution of the governing equations results in large toroidal vortices outside the flame surface. As these naturally formed vortices convect downstream, they force the flame to squeeze at certain locations and bulge at others and cause the flame height to increase and decrease. It is important to note that no artificial perturbation is used in the calculations for the development of these outer vortices. In the presence of gravitational force, acceleration of hot gases along the flame surface generates the vortical structures as part of the solution. Although these vortices (or instabilities) begin to form upstream in the flame near the base region, they develop into recognizable vortical structures only in the locations farther downstream ($z > 50$ mm). However, because of the formation and convection of the vortices, the flame surface oscillates radially at every location, with varying intensity. The

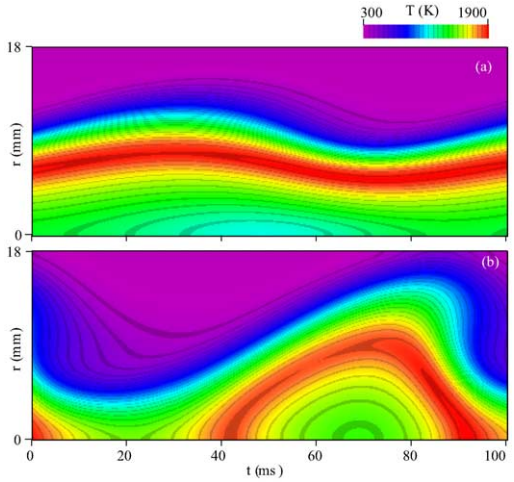

Fig. 2. Temperature evolution obtained at locations (a) 30 mm and (b) 80 mm above burner exit. Flame flicker frequency is ∼ 11 Hz.

frequency corresponding to the passage of these vortices (also known as the flame-flickering frequency) is ∼ 11 Hz. The buoyancy-induced flow entrains the surrounding air into the flame base. The low fuel velocity and the large fuel-cup diameter further increase the entrainment flow which, in turn, generates an inward inclination to the flame surface at the base. As a result, the velocity at the flame base is no longer parallel to the flame surface.

Evolutions of the flame at two different heights above the burner are demonstrated in Fig. 2 through plots of the radial distribution of temperature at different times. While the image in Fig. 1 represents the flame structure for a part of the flame domain at $t = t_0$ ms, that in Fig. 2 represents the temperature at two locations for approximately one cycle ($t_0 + 0\,\text{ms} < t < t_0 + 100$ ms). At $z = 30$ mm, the flame is oscillating radially, along with a weak fluctuation of the fuel jet at the center. However, the vortices formed outside the flame surface have grown significantly by the time they reach a height of 80 mm and pinch off a portion of fuel from the fuel jet. The detached fuel mass burns separately as it convects downstream. A comparison of evolutions at 30 and 80 mm reveals that the period of oscillation at the former location is ∼ 105 ms ($f \sim 9.5$ Hz), while that at the latter is ∼ 93 ms ($f \sim 10.8$ Hz).

4.2. Suppression characteristics under normal gravity

For evaluating the suppression performance of CO_2 in this flame, several calculations were performed by increasing the amount of CO_2 in the air stream while not altering the co-flowing gas velocity

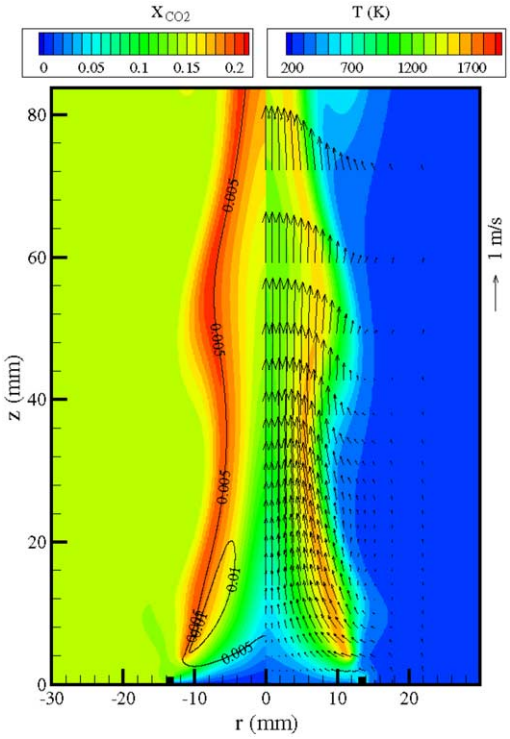

Fig. 3. Structure of normal-gravity flame with near-extinguishment volume fraction (0.145) of CO_2 added to air stream. Temperature and velocity field are shown on right half, and CO_2 and H_2 mole fractions are shown on left half.

at the cup rim. The addition of CO_2 (increase in CO_2 volumetric flow rate) was compensated by a reduction in the volumetric flow rate of air for maintaining the total volumetric flow rate (or velocity) constant. These calculations suggested that when the CO_2 volume fraction was < 10% (i.e., oxygen > 18.9% and nitrogen > 71.1%), no significant change in the flame shape would be observed [15]. For concentrations between 10 and 14.5%, the flame base was separated (< 4 mm) from the burner lip and stabilized at a new location. An instantaneous solution of the computed flame for 14.5% CO_2 is shown in Fig. 3. The variables here are the same as those in Fig. 1. It is evident from this plot that the flame base has moved inside and downstream of the burner lip by ∼ 4 mm. Interestingly, the flame oscillation in the base region increased significantly. As a result, the base of the flame moved back and forth between the burner lip and the location shown in Fig. 3 with time. The separation between the burner lip and the flame base allowed more air and CO_2 to enter the flame and provided partially premixed flow conditions. When the concentration of the added CO_2 was increased to a value > 14.5%, the flame was completely blown out of the computational domain. The experimental result for the extinguish-

ment volume fraction of CO_2 in the air stream was 0.157 ± 0.006 for an oxidizer stream velocity between 2.5 and 18.5 cm/s [24,25]. The calculated extinguishment volume fraction of 14.5% is within 10% of the experimentally obtained value; the agreement seems reasonable considering the complex reaction mechanism incorporated and the approximations used in representing the cup burner with straight tubes in the model.

Calculations made with various CO_2 concentrations indicate that the cup-burner flame extinguishes through the blowoff process, which means that the flame at the base detaches from the burner first (similar to lifting of jet diffusion flames [33]) and then shifts downstream until it clears the computational domain. This suppression-through-blowoff process (i.e., via blowoff process) is the same for all of the cases with CO_2 concentration $> 14.5\%$ and is different from the suppression-through-quenching process in which the flame chemistry is globally turned off by the agent. The latter process is often observed in opposing-flow jet-diffusion-flame configurations in which flames do not posses an edge or base. On the other hand, opposing-flow jet flames are subjected to certain strain rates, depending on the inflow conditions; consequently, the extinguishment concentration for the agent in the opposing-flow jet flame depends on the strain rate applied. For comparing the critical concentrations of CO_2 in extinguishing a cup-burner flame (flame with an edge) and an opposing-jet flame (flame without an edge), calculations were also made for the opposing-jet diffusion flame for two strain-rate conditions. Fuel (pure methane) and air jets issuing from 20-mm-diameter nozzles which are separated by 13 mm are assumed to impinge on each other to create stable opposing-jet diffusion flames. A low strain rate (global) of 30 s^{-1} was achieved by forcing a 0.2 m/s fuel jet toward a 0.2 m/s air jet. Similarly, a moderate global strain rate of 90 s^{-1} was obtained between 0.6 m/s fuel and air jets. Complete axisymmetric 2D simulations (not just 1D along the stagnation line) were made using the CFD code described earlier and adding different concentrations of CO_2 to the air jet.

Several calculations were performed for the two opposing-jet flames by gradually increasing the concentration of CO_2 in the air jet until the flames were extinguished. For the low- and moderate-strain-rate cases, these maximum CO_2 concentrations were found to be 16.4 and 10.4%, respectively. Recently, Bundy et al. [34] obtained extensive data for the suppression limits for various agents (N_2, CO_2, and CF_3Br) using a counterflow burner having 23.4-mm-diameter nozzles and a separation distance of 25 mm. Their data show that the globally strained flames of 30 and 90 s^{-1} were extinguished when 18.7 and 12.5% CO_2 was added to the air stream, respectively. Considering the fact that the nearly double the separation distance used in these experiments (compared with the 13-mm separation used in the present calculations) generates lower local strain rates at the flame surface due to jet expansion, which, in turn, demand larger amounts of agent for flame extinguishment, they compare reasonably well with the respective measurements of Bundy et al. [34].

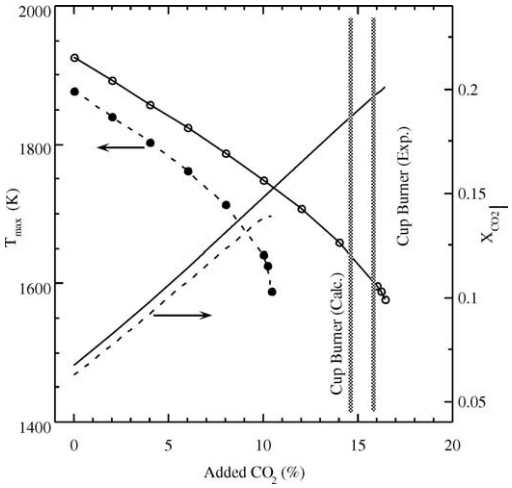

Fig. 4. Variations in flame temperature (T_{max}) and peak CO_2 mole fraction with percentage of CO_2 added to air in opposing-jet diffusion flames. (Solid and dashed lines represent 30 and 90 s^{-1} stretched flames, respectively.) Computed and measured limiting concentration for cup burner are indicated by vertical bars.

The critical agent concentration obtained for the cup-burner flame is compared with those obtained for the opposing-jet flames in Fig. 4. The variations in flame temperature and peak CO_2 produced in the flame zone as functions of added CO_2 are shown for the two opposing-jet flames with different strain rates (30 and 90 s^{-1}). The temperature of the weakly strained flame with 0% CO_2 added is slightly higher than that of the cup-burner flame; the temperature of the moderate-strain flame is slightly lower. Consistent with these temperatures, the limiting volume fraction of CO_2 for the cup burner (14.5% computed) falls between those of the two opposing-jet-flame cases, but nearer the critical volume fraction (16.4%) of the low-strain opposing-jet flame. This result is indeed consistent with the experimental observations that the extinguishment concentrations for the cup-burner flames are generally comparable to those for opposing-jet flames at low strain rates (~ 50 s^{-1}) [35,36]. Interestingly, both opposing-jet flames extinguished at ~ 1580 K, which indicates that the suppression of opposing-jet diffusion flames is controlled primarily by kinetics, as was observed experimentally [37].

4.3. Flame structure under microgravity

The gravitational force acting on the cup-burner flames in Figs. 1 and 3 caused the flow to accelerate and induced flow instabilities. Earlier studies on jet diffusion flames in microgravity [16–18,38,39] suggest that flames tend to become steady in nature and larger in diameter as the gravitational force on them decreases. To investigate the effects of gravitational force on cup-burner flames, calculations were repeated under various gravitational force conditions. Results for $0.5g$, $0.2g$, $0.1g$, and $0g$ are shown in Figs. 5a–5d, respectively. Mole fractions of CO_2 and H_2 are shown on the left half in these figures, while the velocity field and temperature are shown on the right. Note that the contour legends, color tables, and velocity-vector magnitudes used in these figures are identical to those used for the $1g$ flame (Fig. 1).

The salient features noted from a comparison of flame structures obtained under various gravitational force conditions are: (1) the flames became steady-state when the gravitational acceleration was $< 0.5g$; (2) the flame height and diameter increased with a reduction in gravitational force; (3) the peak velocity at a height of 80 mm above the burner decreased from ~ 2.2 to ~ 0.2 m/s when gravity was reduced from $1g$ to $0g$; (4) the maximum temperature decreased slightly but, more importantly, the temperature of the flame tip decreased dramatically with a reduction in gravitational force; and (5) the severely concave (with respect to the burner) flame near the burner rim became parallel to the fuel jet when the gravitational force was reduced from $1g$ to $0g$.

Several investigators have studied the relationship between flame flicker and gravitational force [26,40]. In general, flames were found to oscillate, even under very low gravity conditions. It was suggested that the flicker frequency increases with gravitational force raised to a power, typically, 0.5. Contrary to these findings, flicker appears to cease in cup-burner flames when the gravitational acceleration is reduced to $0.5g$. Several attempts with smaller time steps and finer grids failed to produce a flickering flame for $0.5g$. This suggests that buoyancy-induced instability possesses a cutoff value on the gravitational force scale below which it vanishes. This is characteristic of an absolute instability mode of a jet flow [41]. In a typical jet diffusion flame with a small-diameter nozzle and high-velocity fuel jet, the cutoff gravitational force for the disappearance of the absolute-instability mode is near zero and was not captured either in the calculations or in the experiments. However, the very low fuel-jet velocity and the large-diameter fuel cup used in the present investigation appear to increase the limiting value to $0.5g$. The existence of such a limiting value for the flame oscillations further confirms that the buoyancy-induced instabilities are of the absolute-instability type.

The flame structure shown in Fig. 5d for the $0g$ case represents an open-tipped flame [39,42]. In fact, decreasing the gravitational force on a cup-burner flame produced dramatic changes in its structure. At $1g$, the flame was severely oscillating, with packets of fuel being pinched off from the jet and burning independently (Figs. 1 and 2). At $0.5g$, a closed-tip steady-state flame was generated (Fig. 5a). Even though the temperature of the flame tip under a gravitational acceleration of $0.2g$ decreased significantly, the flame tip was still closed at the centerline (Fig. 5b). Finally, for $0.1g$ and $0g$ conditions the flames became open-tipped ones, with burning taking place only in the shoulder regions (Figs. 5c and 5d).

The maximum heat release rate, its radial location, and the flame temperature at different heights in the flame for various gravitation forces are shown in Figs. 6a–6c, respectively. The heat release rate in laminar flames such as those in Fig. 5 represents the local chemical reactivity, and the radial location of the peak value represents half the flame diameter. As Fig. 6b shows, the diameter of the flame increases with a decrease in gravitational force. Interestingly, the flame height decreased when the gravitational acceleration was reduced from $0.5g$ to $0.2g$. Earlier studies have indicated that flame height may increase with gravitational force in some flames [17,26] and may decrease in others [39,42]. Apparently, the fuel-jet velocity has an important effect on the flame height with decreasing gravitational force: the flame height of the higher-jet-velocity flame [17] decreases and that of the lower-jet-velocity flame [39] increases when the gravitational force is decreased.

Distributions of the peak heat release rate in Fig. 6a and flame temperature in Fig. 6c demonstrate the tip-opening process taking place in microgravity flames. In general, the heat release rate and flame temperature decrease when the gravitational force is reduced, and more interestingly, the latter quantity decreases with height more rapidly in lower-gravity flames. It was found from earlier calculations [43] that methane/air opposing-jet diffusion flames quench when the flame temperature drops below 1500 K. Based on this criterion, as the flame temperature under $0.1g$ and $0g$ conditions dropped below 1500 K for heights greater than 74 and 40.5 mm, respectively, flames downstream of these locations should be considered quenched. As flame quenching occurs when r_f is > 0 (Fig. 6b), these flames could be referred as open-tipped ones. On the other hand, under $0.5g$ and $0.2g$ conditions, flame temperature was above 1500 K before the flame surfaces crossed the centerline, and hence, these flames could be referred

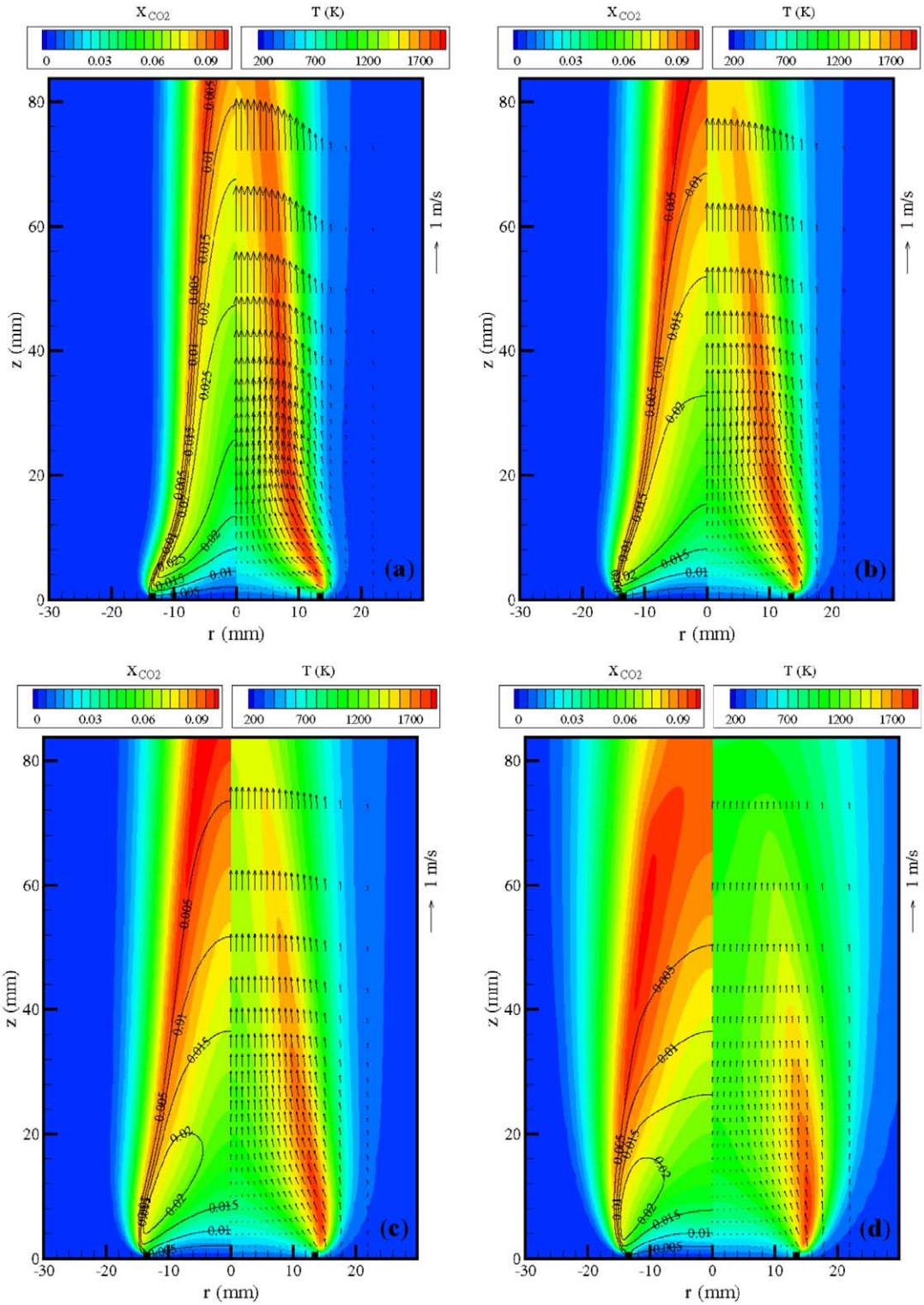

Fig. 5. Cup-burner flames under (a) $0.5g$, (b) $0.2g$, (c) $0.1g$, and (d) $0g$ conditions. Temperature and velocity fields are shown on right halves, and CO_2 and H_2 mole fractions are shown on left halves.

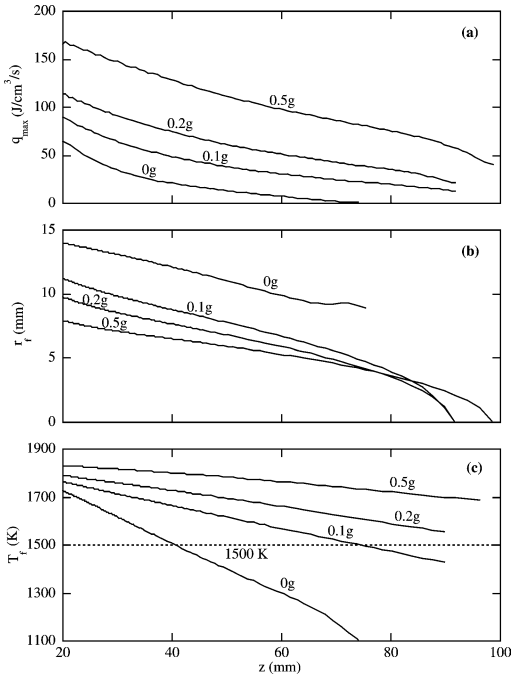

Fig. 6. Axial distributions of peak heat release rate $q_{\max}$ and flame radius r_f (lines with symbols) under various gravitational conditions.

as closed-tip ones. The reasons for flame opening appearing in lower-g cases is discussed in the next section.

A different conclusion on tip opening emerges if one considers zero heat release rate as quenching criterion. As seen from Figs. 6b and 6c, heat release rate does not reduce to zero value when the flame temperature decreases to the quenching value of 1500 K. The chemical reactivity in the mixing region between the products and air releases residual heat, and local heat release rate becomes zero only when all the chemical reactivity is quenched. One might assume that the tip of the flame is absolutely opened when the peak heat release rate decreases to zero before the flame surface converges to the centerline. For gravitational accelerations of $0.1g$, $0.2g$, and $0.5g$, flame surfaces intersect with the centerline and the local heat release rates at the flame tips are 13, 21, and 40 J/(cm^3 s), respectively (Fig. 6a). Based on the zero heat release rate criterion these flames could be considered as closed-tip ones. On the other hand, in $0g$ flame the peak heat release rate approached zero when the flame surface was still at 8.9 mm from the centerline, representing an absolutely opened flame tip. It is important to recall that based on quenching-temperature criterion both the $0g$ and $0.1g$ flames were considered as opened-tip ones.

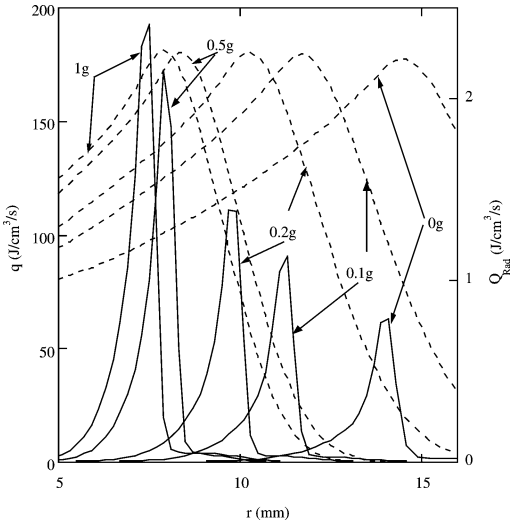

Fig. 7. Distributions of heat release rate q (solid lines) and radiative heat loss Q_{rad} (broken lines) at 20 mm above burner under various gravitational conditions.

4.4. Importance of radiation under microgravity

As described earlier, radiation from CO_2, H_2O, CO, and CH_4 was included in the present calculations. A simple radiation model based on the optically thin medium assumption was employed. As suggested by Bonne [44] and T'ien [45], radiative heat losses could become a dominating heat transfer mechanism when the generation of heat is decreased because of the lack of reactant convection in microgravity. To verify this, radial distributions of the heat release rate and the radiative heat loss at 20 mm above the burner were plotted (Fig. 7) for various g cases. At this height the flame exists in all g cases. Fig. 7 shows that the heat release rate decreases significantly with a reduction in gravitational force. For the $0g$ case the maximum heat release rate is only one-third that obtained for the $1g$ case. As flame temperatures are approximately the same at this location for all of the cases, the reduction in heat release rate can be attributed to the reduction in reactant fluxes into the flame zone. The drastic decrease in convective flow in the $0g$ case limits the reactant fluxes into the flame zone in the downstream locations. On the other hand, the local radiative heat losses are about the same in all g cases. Note that the total radiative heat loss integrated over the entire flame may increase as the flame becomes larger under low-gravity conditions. The dominance of local radiative heat loss over heat release rate in the $0g$ case causes the flame to quench at the tip locations, where the heat release rate is smaller. The fuel and oxidizer fluxes in the vicinity of the flame surface are compared in Fig. 8 for normal-gravity (left) and zero-gravity (right) conditions. The

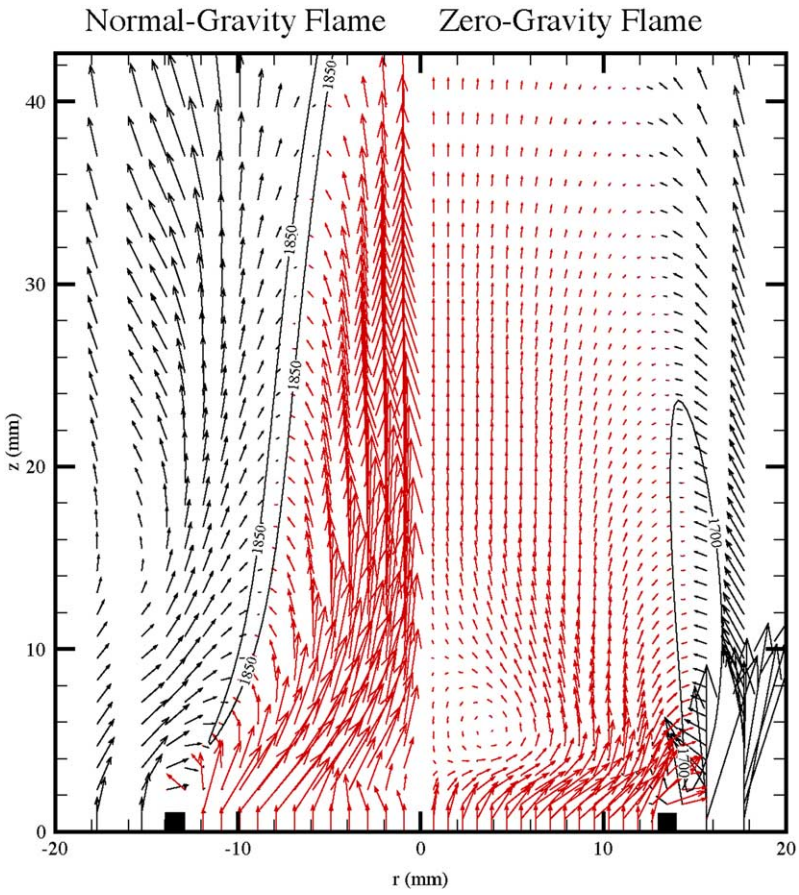

Fig. 8. Fuel and oxidizer fluxes under normal-gravity (left) and zero-gravity (right) conditions.

flame surface locations are identified by plotting near-peak-temperature contours. It is evident from this plot that the amount of fuel and oxygen penetrating into the combustion products has significantly decreased under zero-gravity conditions. In the presence of radiative heat loss, this reduction in mixing could not maintain the flame temperature above the quenching limit; hence, flame extinction occurred at downstream locations.

To further verify that the radiative heat losses are causing the flame to extinguish at the tip, numerical experiments were performed on a $0g$ flame. Three calculations were made for this flame, ignoring (1) radiation in the energy equation, (2) finite-rate chemistry, and (3) both radiative heat loss and finite-rate chemistry. The flow conditions and numerical details used for these calculations were the same as those employed for the flame ($0g$ case) shown in Fig. 5d. All three calculations converged to steady-state flames, even though unsteady simulations were performed.

The $0g$ flame computed with no radiation is shown in Fig. 9; the plotting scheme employed is the same as that used for Fig. 5d. As expected, in the absence of radiation, the flame tip closed and burning took place along the flame surface from the base at the burner rim to the tip at the centerline. The peak flame temperature increased by ~ 150 K; however, more interestingly, all along the flame surface, the temperature was constant. The closed contours of H_2 in Fig. 5d have disappeared in Fig. 9, indicating that combustion is taking place all the way up to the flame tip when the radiation is turned off in the calculations. Because of this increased burning (and volumetric expansion), the local velocity has increased by $\sim 35\%$ at $z = 80$ mm, compared with that in the $0g$ flame without radiation (shown in Fig. 5d).

Flames resulting from the calculations made using the infinitely fast one-step chemical-kinetic model ($CH_4 + 2O_2 + 7.5N_2 \Rightarrow CO_2 + 2H_2O + 7.5N_2$) are shown in Fig. 10. The iso-temperature color plots of the flames without and with radiation are shown in the left and right halves, respectively. The temperature fields of these flames became similar to those of their counterparts that were computed with finite-rate (detailed) chemistry. The infinitely fast chemistry flame computed with radiation is similar to that shown in

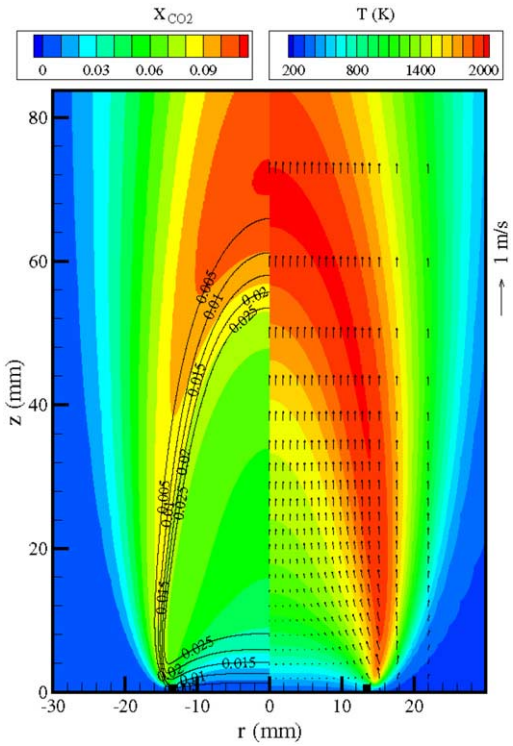

Fig. 9. Cup-burner flame under 0g conditions, calculated by ignoring radiative heat losses.

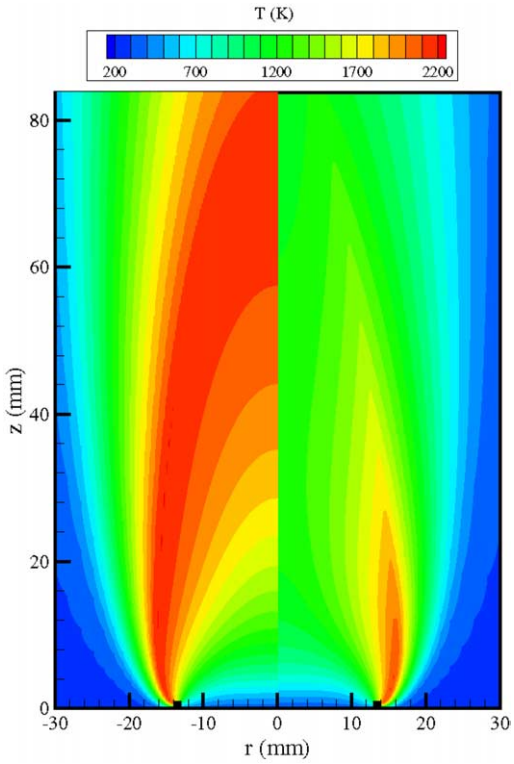

Fig. 10. Cup-burner flame under 0g conditions, calculated with infinitely fast chemical kinetics. Flames without and with radiative heat losses are shown in left and right halves, respectively.

Fig. 5d, and the flame computed without the radiative heat loss is similar to that shown in Fig. 9 (right side). These comparisons further suggest that finite-rate chemistry is not responsible for the tip quenching observed in the 0g and low-g flames; rather, the flame quenching results from the deficiency of reactants. Calculations were also performed with detailed chemistry for the 0g flame using the unity Lewis number assumption (not shown). The resulting flame with radiative heat loss has a structure similar to that shown in Fig. 5d. This suggests that neither curvature nor preferential diffusion is responsible for the tip opening of the 0g flame. Analysis of the results obtained from the various numerical experiments suggests that radiative heat losses are predominantly responsible for the quenching phenomenon observed in microgravity cup-burner flames. Interestingly, similar numerical experiments performed on jet diffusion flames established with a 1-cm-diameter nozzle and high fuel-jet velocities under zero-gravity conditions suggested that radiation has a negligible effect on the flame structure. Therefore, other factors such as low fuel velocity and large fuel-tube diameter associated with the cup-burner flames might have also contributed to the tip-quenching phenomenon observed under microgravity conditions.

To understand why radiation affected only the low-g flames, calculations for the 1g flame were also repeated with the radiative heat loss in the energy equation being turned off. The flame resulting from this simulation is shown in Fig. 11; the plotting scheme adopted for Fig. 1 was used. Although some minor differences exist in the flame temperatures, overall the 1g flames obtained with (Fig. 1) and without (Fig. 11) the radiative heat losses are similar in structure. The tips of both flames are closed, with burning taking place all along the flame surface. Both flames are flickering, which results in pinching off of the fuel packets at the tip. However, the flickering frequency increased to 12.5 Hz when the radiative heat loss was ignored in the calculations. An additional vortex seems to be forming in Fig. 11 compared with those formed in Fig. 1. These differences in flame dynamics should be expected because the buoyancy forces increase slightly with an increase in flame temperature in Fig. 11.

The temperature and axial velocity along the flame surface obtained with and without radiation are plotted for the 0g flame in Fig. 12a and for the 1g flame in Fig. 12b. In all four calculations, temperature and ax-

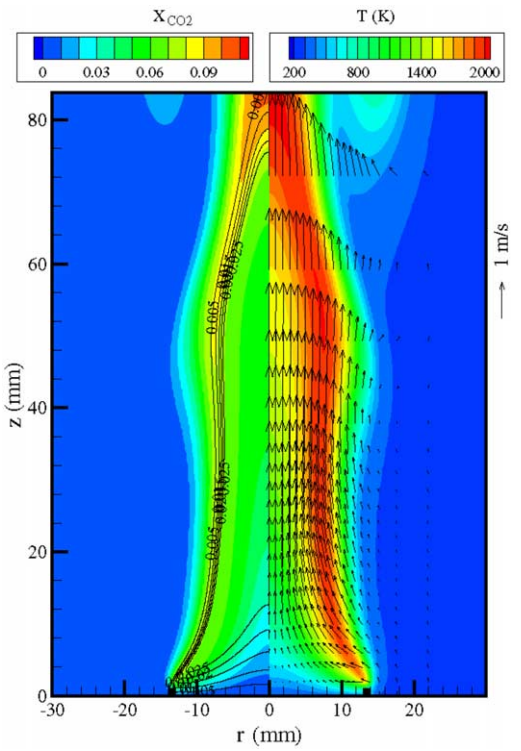

Fig. 11. Cup-burner flame under normal-gravity conditions, calculated by ignoring radiative heat losses.

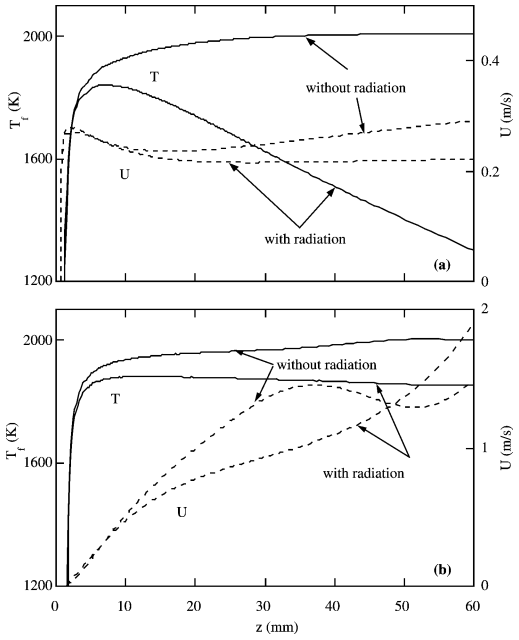

Fig. 12. Variations of temperature and axial velocity with height along flame surface for (a) 0g and (b) 1g flames.

ial velocity have increased initially in the flame base region. However, in the 0g case, flame temperature remained more or less constant around 2000 K in the downstream locations when radiation was ignored in the calculations and decreased linearly from 1850 K when radiation was included. Based on the quenching temperature of 1500 K [43], it can be assumed that the 0g flame (computed with radiative heat loss) is quenched at locations $z > 40.5$ mm. Absence of combustion (or volumetric expansion) in these locations resulted in a constant axial velocity of ~ 0.22 m/s, whereas axial velocity increased monotonically when the radiation was not considered. Note that the starting location for quenching determined based on a 1500 K temperature criterion is different from that obtained using the zero heat release rate criterion (Fig. 6).

In the case of the 1g flame, calculations made with and without the radiative heat losses yielded flame temperatures that are nearly constant (Fig. 12b). In both of these 1g calculations the axial velocity has increased rapidly with z, primarily due to buoyancy and, to some extent, due to thermal expansion of the hot gases. The oscillations in the axial velocity resulted from the squeezing and bulging actions of the convecting vortices (cf. Figs. 1 and 11). The higher axial velocities in the case of the 1g flame (~ 1 m/s compared with 0.22 m/s in the 0g case) resulted in higher reactant fluxes into the flame zone and, in turn, increased heat release rates, sufficiently high to overcome the heat losses due to radiation. As a result, radiation had a negligible effect on the 1g flame. The weak axial velocity in 0g flames, on the other hand, brought significantly smaller amounts of reactants into the flame zone. While these lowered reactant fluxes could be able to maintain a flame in the absence of radiative heat losses, they failed in doing so when part of the heat generated in the flame zone was removed due to radiation. Consequently, one should not expect flame quenching in the tip region in 0g if the fuel-jet velocity is sufficiently high.

4.5. *Flame-suppression characteristics under* 0g

Calculations made for 1g and 0g conditions revealed dramatic differences in the flame structures, due mainly to buoyancy and radiation. Because of these differences, suppression of the 0g flame through injection of CO_2 into the air stream could differ from that of the 1g flame shown in Figs. 3 and 4. To evaluate the performance of CO_2 in extinguishing 0g flames, several calculations were made by adding CO_2 in various volume fractions to the air stream of the 0g flame shown in Fig. 5d. The limiting volume fraction of CO_2 required to extinguish the flame was found to be 19.1%. This limiting value is nearly 32% higher than that required for extinguishing the same flame under normal-gravity conditions. Results ob-

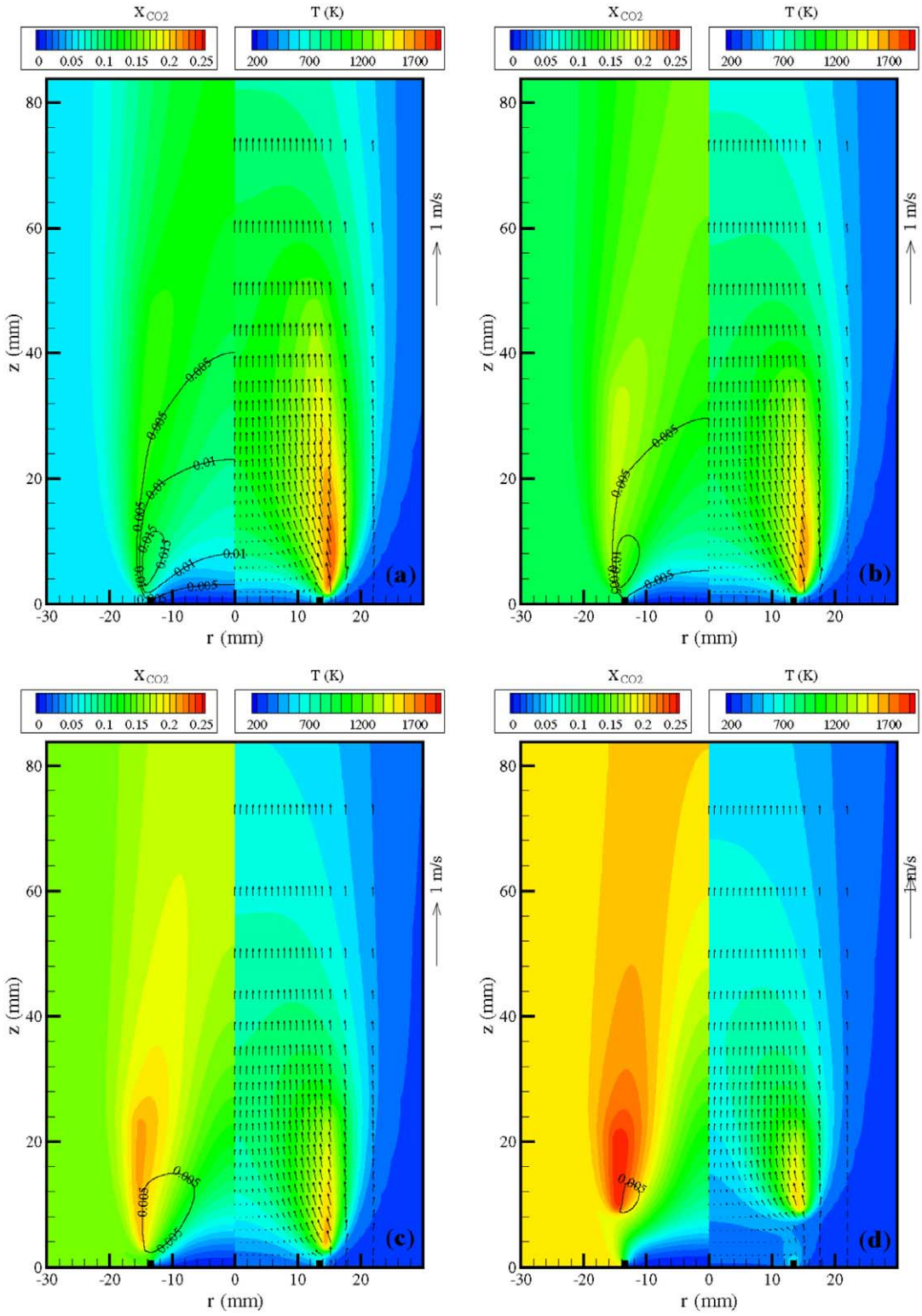

Fig. 13. Effect of CO_2 addition to airflow on $0g$ cup-burner flame. CO_2 addition: (a) 5%, (b) 10%, (c) 15%, (d) limiting value of 19.1%. Temperature and velocity fields are shown on right half, and CO_2 and H_2 mole fractions are shown on left half.

tained with 5, 10, 15, and 19.1% CO_2 are shown in Fig. 13. The plotting scheme used here is the same as that employed for Fig. 3. The addition of CO_2 did not change the overall structure of the $0g$ flame. That is, irrespective of the amount of CO_2 added, the flame tip was opened, and the entire flame remained vertical. However, as the CO_2 volume fraction was increased, the height of the vertical flame also decreased.

Similar to the $1g$ flame quenching process, the primary role of CO_2 in $0g$ flame quenching was to destabilize the flame base. As CO_2 was added to the air stream, the flame became weaker and the temperature in the base region decreased. For smaller volume fractions (< 0.1) of CO_2, the location of the peak temperature (within the flame base) moved upstream, toward the burner rim; for moderate volume fractions ($0.1 < X_{CO_2} < 0.15$), it moved slightly downstream, away from the burner rim. When the CO_2 volume fraction was increased beyond 15%, the peak temperature location shifted downstream and yet the flame sought a new stabilization location in the flowfield. For volume fractions $> 19.1\%$, the flame base became unstable and continued to move downstream in search of a new stabilizing location. Because the flame failed to find another stabilizing location, it was completely removed from the computational domain, resulting in flame suppression via blowoff. As in the $1g$ case, the flame at $0g$ did not extinguish before its base became unstable.

The location of the peak temperature within the flame base and the value of the peak temperature are plotted in Fig. 14 for the $1g$ case and in Fig. 15 for the $0g$ case for various concentrations of CO_2. The limiting volume fractions of CO_2 necessary for extinguishing these flames are also shown. The flame base locations identified from visible blue light in the experiment and from the lowest point of the 1500 K temperature contour in the calculations are also shown in Fig. 14. The predicted flame base movement with added CO_2 agrees qualitatively with that obtained in the experiment. In both the calculations and experiments flame base shifted very little when the added CO_2 volume fraction was less than 12% and shifted more quickly for higher CO_2 concentrations. Note that the calculations slightly underpredict the limiting volume fraction for extinguishing the cup-burner flame. The computed flame base movement for the case of the $0g$ flame is shown in Fig. 15; corresponding experiments employing the NASA drop tower are in progress.

The suppression mechanisms of the $1g$ and $0g$ flames, as evident from Figs. 14 and 15, are similar. In both flames the peak temperature location was nearer the burner rim initially and then moved away with increased CO_2 volume fraction in the co-flow stream. On the other hand, the peak temperature in the flame base decreased monotonically with CO_2 concentration. Some differences can be observed between the extinguishing processes taking place under $0g$ and $1g$ conditions. First, the peak temperature location under the $1g$ condition is more sensitive to the volume fraction of the added CO_2. This is probably due to the higher velocities near the flame base that are induced from the strong entrainment present in these buoyant flames. Second, the peak temperature prior to extinguishment decreased rapidly in the case of the $1g$ flame but decreased linearly in the case of the $0g$ flames. A rapid decrease in flame temperature near extinguishment was also observed in the higher strain-rate case of opposing-jet diffusion flames (Fig. 4). It is interesting to note that the bases of the $1g$ flame and the opposing-jet flame are subjected to stretching, whereas the base of the $0g$ flame remains nearly unstretched. This means that the rapid

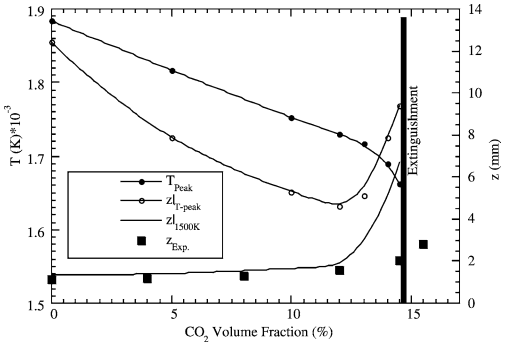

Fig. 14. Peak temperature within base region, its location with respect to burner rim, and location of leading edge of 1500 K contour with respect to burner rim for various volume fractions of CO_2 in air stream for $1g$ flame. Solid square symbols represent visible flame-base location obtained in experiments.

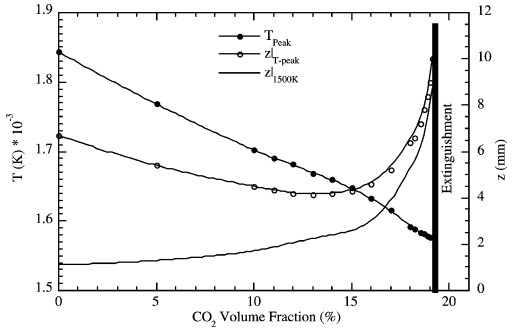

Fig. 15. Peak temperature within the base region, its location with respect to burner rim, and location of leading edge of 1500 K contour with respect to burner rim for various volume fractions of CO_2 in air stream for $0g$ flame.

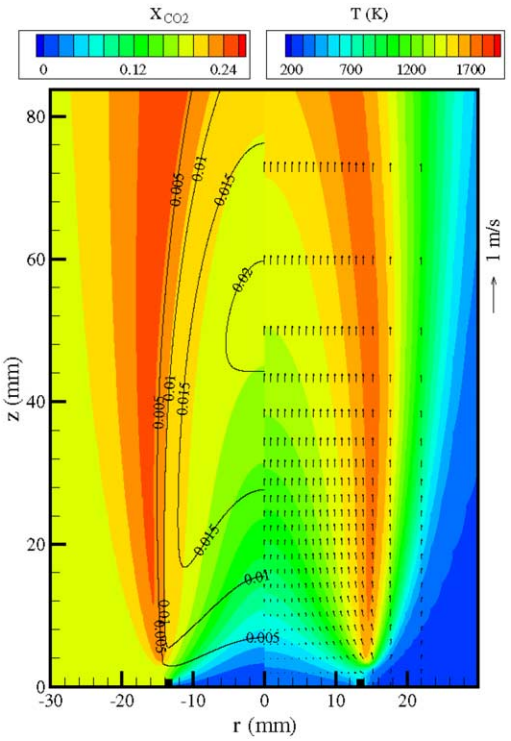

Fig. 16. Cup-burner flame under $0g$ conditions and with 19.1% CO_2 added to air stream. Calculations were made after ignoring radiative heat losses. Temperature and velocity fields are shown on right half, and CO_2 and H_2 mole fractions are shown on left half.

decrease in flame temperature near extinguishment that is observed in ground-based experiments and in opposing-jet flames is due to the inherent stretch present on these flames and that only in microgravity can one find true limits (unaffected by stretch) for extinguishment.

To determine the effect of radiation on the near-extinguishment flame structure (Fig. 11d), calculations for the $0g$ flame with 19.1% CO_2 added in the air stream were repeated, with the radiative heat losses in the energy equation turned off. The resulting flame is shown in Fig. 16; the plotting scheme is adopted from that used in Fig. 13d. When the radiative heat loss was ignored, the tip of the flame became closed, with burning taking place all along the flame surface between the burner rim and the centerline. The flame base also moved toward the burner rim (cf. Figs. 16 and 13d), representing a more stable flame. This means that the extinguishment limit obtained by ignoring radiation would be $> 19.1\%$. It also illustrates the importance of considering radiation when the extinguishment limits are being determined.

5. Conclusions

A pure methane–air diffusion flame formed over a cup burner was used to explore the suppression characteristics of CO_2 under normal- and microgravity conditions. A detailed chemical-kinetic model GRI-V1.2 having 31 species and 346 elementary reaction steps was incorporated into a time-dependent, axisymmetric CFD model for investigation of the effects of CO_2 on methane combustion. Under normal-gravity conditions, the laminar cup-burner flame for a low fuel flow rate and a low-speed annular airflow generated large-scale, low-frequency (~ 11 Hz) organized vortices on the air side of the flame. Calculations were performed for this flame under various gravitational forces. It was observed that the cup-burner flame ceases to flicker for gravitational levels $< 0.5g$. As the buoyancy forces were reduced, the flame diameter increased, the tip of the flame extinguished (opened), and the flame at the base became vertical. Through numerical experiments it was found that radiative heat loss was predominantly responsible for the extinguishment of the flame tip under $0g$ conditions. On the other hand, ignoring radiation in the $1g$ flame calculation did not change the burning characteristics along the flame surface, however, it resulted in a 25% increase in the flicker frequency.

Calculations for the cup-burner flame were made by adding CO_2 to the air stream for obtaining the limiting volume fraction for extinguishing the $1g$ and $0g$ flames. The predicted flame base movement with added CO_2 agrees qualitatively with that obtained in the experiment in $1g$. In both the calculations and experiments flame base shifted very little when the added CO_2 volume fraction was less than 12% and shifted more quickly for higher CO_2 concentrations. The predicted limiting volume fraction of 14.5% for the cup burner under $1g$ conditions is within 10% of the measured value. For comparison purposes, suppression limits for a weakly strained and for a moderately strained opposing-jet diffusion flame were also obtained. Under $1g$ conditions, the limiting CO_2 volume fraction for the cup burner is found to be between those of the two opposing-jet flames.

Similar to the case of the $1g$ flames, the addition of CO_2 to $0g$ flames destabilized the flame base, which then moved downstream in search of a new stabilization location. For CO_2 volume fractions $> 19.1\%$, the flame base moved out of the computational area as it could not find a stabilization point within this domain. This limiting concentration for the $0g$ flame is $\sim 32\%$ higher than that obtained for the same flame under normal-gravity conditions. Calculations made by ignoring radiation for the limiting flame under $0g$ conditions yielded a stable flame. It is important to

consider radiation when estimating the extinguishment limits of cup-burner flames in microgravity.

Acknowledgments

This work was supported by the Office of Biological and Physical Research, NASA, Washington, DC. The first author thanks Dr. Mel Roquemore of the Air Force Research Laboratory for stimulating discussions on buoyant flames. The authors acknowledge Marian Whitaker for editorial assistance.

References

[1] S.O. Anderson, Fire J. 81 (1987) 56–118.
[2] R.G. Gann (Ed.), Halogenated Fire Suppressants, ACS Symposium Series, vol. 16, American Chemical Society, Washington, DC, 1975.
[3] J.C. Biordi, C.P. Lazzara, J.F. Papp, Combust. Flame 23 (1974) 73–82.
[4] C.K. Westbrook, Combust. Sci. Technol. 34 (1983) 201–225.
[5] M.R. Nyden, G.T. Linteris, D.R.F. Burgess Jr., P.R. Westmoreland, W. Tsang, M. Zachariah, in: W.L. Grosshandler, R.G. Gann, W.M. Pitts (Eds.), Evaluation of Alternative In-Flight and Dry Bays, in: NIST SP, vol. 861, National Institute of Standards and Technology, Gaithersburg, MD, 1994, p. 467.
[6] G.T. Linteris, L. Truett, Combust. Flame 105 (1/2) (1996) 15–27.
[7] G.T. Linteris, D.R. Burgess Jr., V. Babushok, M. Zachariah, W. Tsang, P. Westmoreland, Combust. Flame 113 (1/2) (1998) 164.
[8] K. Prasad, C. Li, K. Kailasanath, C. Ndubizu, R. Ananth, P.A. Tatem, Combust. Sci. Technol. 132 (1–6) (1998) 325.
[9] T.A. Milne, C.L. Green, D.K. Benson, Combust. Flame 15 (1970) 255–264.
[10] K. Seshadri, N. Ilincic, Combust. Flame 101 (1995) 271–294.
[11] A. Abbud-Madrid, J.T. McKinnon, S. Gokoglu, in: K. Sacksteder (Ed.), Proceedings, Seventh International Workshop on Microgravity Combustion and Chemically Reacting Systems, 2003, pp. 281–284, NASA/CP-2003-212376.
[12] National Fire Protection Agency, Standard on Clean Agent Fire Extinguishing Systems, NFPA 2001, 2000.
[13] B. Hirst, K. Booth, Fire Technol. 13 (1977) 296.
[14] G.T. Linteris, G.W. Gmurczyk, in: R.G. Gann (Ed.), Fire Suppression System Performance of Alternative Agents in Aircraft Engine and Dry Bay Laboratory Simulations, National Institute of Standards and Technology, Gaithersburg, MD, 1995.
[15] V.R. Katta, F. Takahashi, G.T. Linteris, in: D.D. Evans (Ed.), Fire Safety Science—Proceedings of the Seventh International Symposium, International Association for Fire Safety Science, 2002, pp. 531–542.
[16] U. Hegde, L. Zhou, Y.M. Bahadori, Combust. Sci. Technol. 102 (1994) 95.
[17] V.R. Katta, L.P. Goss, W.M. Roquemore, AIAA J. 32 (1) (1994) 84–94.
[18] F. Takahashi, V.R. Katta, Proc. Combust. Inst. 29 (2002) 2509–2518.
[19] J.L. Ellzey, K.J. Laskey, E.S. Oran, in: A.L. Kahl, J.C. Leyer, A.A. Borisov, W.A. Sirgnano (Eds.), Dynamics of Deflagrations and Reactive Systems: Flames, in: Progress in Astronautics and Aeronautics, vol. 131, American Institute of Aeronautics and Astronautics, Reston, VA, 1989, p. 179.
[20] R.W. Davis, E.F. Moore, W.M. Roquemore, L.D. Chen, V. Vilimpoc, L.P. Goss, Combust. Flame 83 (3/4) (1991) 263–270.
[21] C.R. Kaplan, E.S. Oran, K. Kailasanath, H.D. Ross, Proc. Combust. Inst. 23 (1996) 1301–1308.
[22] T. Takagi, Z. Xu, Combust. Flame 96 (1/2) (1994) 50–59.
[23] V.R. Katta, W.M. Roquemore, Combust. Flame 100 (1) (1995) 61–70.
[24] F. Takahashi, G. Linteris, V.R. Katta, in: Proceedings of the Fourth International Symposium on Scale Modeling (ISSM-IV), Cleveland, OH, September 2003.
[25] G.T. Linteris, V.R. Katta, F. Takahashi, Combust. Flame (2003).
[26] W.M. Roquemore, V.R. Katta, J. Visualization 2 (3/4) (2000) 257–272.
[27] M. Frenklach, H. Wang, M. Goldenberg, G.P. Smith, D.M. Golden, C.T. Bowman, R.K. Hanson, W.C. Gardiner, V. Lissianski, Technical Report No. GRI-95/0058, Gas Research Institute, Chicago, IL, November 1, 1995.
[28] Computational Submodels, International Workshop on Measurement and Computation of Turbulent Nonpremixed Flames., http://www.ca.sandia.gov/TNF/radiation.html, 2003.
[29] V.R. Katta, L.P. Goss, W.M. Roquemore, Int. J. Numer. Methods Heat Fluid Flow 4 (5) (1994) 413–424.
[30] V.R. Katta, K.Y. Hsu, W.M. Roquemore, Proc. Combust. Inst. 27 (1998) 1121–1127.
[31] V.R. Katta, C.D. Carter, G.J. Fiechtner, W.M. Roquemore, J.R. Gord, J.C. Rolon, Proc. Combust. Inst. 27 (1998) 587–594.
[32] V.R. Katta, W.M. Roquemore, AIAA J. 36 (11) (1998) 2044–2054.
[33] F. Takahashi, V.R. Katta, Proc. Combust. Inst. 28 (2000) 2071–2078.
[34] M. Bundy, A. Hamins, K.Y. Lee, Combust. Flame 133 (3) (2003) 299–310.
[35] A. Hamins, D. Trees, K. Seshadri, H.K. Chelliah, Combust. Flame 99 (2) (1994) 221–230.
[36] F. Takahashi, W.J. Schmoll, E.A. Strader, V.M. Belovich, Combust. Sci. Technol. 163 (2001) 107–130.
[37] S. Ishizuka, H. Tsuji, Proc. Combust. Inst. 18 (1981) 692–695.
[38] D.L. Urban, Z.G. Yuan, P.B. Sunderland, G.T. Linteris, J.E. Voss, K.C. Lin, Z. Dai, K. Sun, G.M. Faeth, AIAA J. 36 (8) (1998) 1346–1360.

[39] P.B. Sunderland, B.J. Mendelson, Z.G. Yuan, D.L. Urban, Combust. Flame 116 (3) (1999) 376–386.
[40] M.Y. Bahadori, L. Zhou, D.P. Stocker, U. Hegde, in: Proceedings, 1996 Fall Technical Meeting of the Eastern States Section of the Combustion Institute, Combustion Institute, Pittsburgh, PA, 1996, pp. 451–454.
[41] S. Raghu, P. Monkewitz, Phys. Fluids A 3 (4) (1991) 501–503.
[42] K.C. Lin, G.M. Faeth, P.B. Sunderland, D.L. Urban, Z.G. Yuan, Combust. Flame 116 (4) (1999) 415–431.
[43] V.R. Katta, W.M. Roquemore, in: Combustion Fundamentals and Applications: Proceedings of the Central States Section of the Combustion Institute, Combustion Institute, Pittsburgh, PA, 1996, pp. 449–454.
[44] U. Bonne, Combust. Flame 16 (1971) 147–159.
[45] J.S. T'ien, Combust. Flame 65 (1986) 31–34.